Ultrafast laser-induced crystallization of amorphous silicon films

Tae Y. Choi
Swiss Federal Institute of Technology Zurich
Institute of Energy Technology
CH-8092, Switzerland

David J. Hwang
Costas P. Grigoropoulos
University of California
Department of Mechanical Engineering
Berkeley, California 94720-1740
E-mail: djhmech@newton.berkeley.edu

Abstract. Ultrashort pulsed laser irradiation is used to crystallize 100-nm amorphous-silicon (a-Si) films. The crystallization process is observed by time-resolved pump-and-probe reflection imaging in the range of 0.2 ps to 100 ns. The *in-situ* images, in conjunction with postprocessed scanning electron microscopy (SEM) and atomic force microscopy (AFM) mapping of the crystallized structure, provide evidence for nonthermal ultra-fast phase transition and subsequent surface-initiated crystallization. © 2003 Society of Photo-Optical Instrumentation Engineers.
[DOI: 10.1117/1.1617312]

Subject terms: ultrashort; amorphous silicon; pump and probe; ultrafast phase transition; crystallization.

Paper 030015 received Jan. 9, 2003; revised manuscript received May 19, 2003; accepted for publication May 19, 2003.

1 Introduction

Pulsed laser-induced crystallization of thin semiconductor films on amorphous substrates has major applications in the fabrication of thin film transistors (TFTs) for high-definition active matrix liquid crystal displays (AMLCDs).[1] Typically utilized nanosecond pulses crystallize amorphous-silicon (a-Si) films via a rapid melting and solidification process. The associated energy transfer and phase-change thermodynamics have been studied by a variety of *in-situ* diagnostics[2] of nanosecond temporal resolution, including time-resolved optical transmission, reflection, multiwavelength emission, and transient electrical conductance measurements. It was found that the crystallized material structure critically depends on the laser fluence (i.e., the pulse energy per unit surface area) and the melt quench rate that is determined by the heat loss to the substrate.

The melt-mediated crystallization is contrasted with plasma annealing. Femtosecond laser excitation of semiconductors is assumed to initiate ultrafast phase transition via the plasma annealing mechanism.[3,4] A high level of electronic excitation can severely weaken interatomic bonds so that "cold" atomic motion can lead to disordering of the lattice. The ultrafast transition caused by the high-density electron hole plasma inherently carries no conventional molten phase. Investigations utilizing femtosecond time-resolved optical microscopy and reflectivity measurements[5–7] suggested existence of a liquid layer whose properties and transient behavior differ from normal thermal melting. Experiments[8–10] and theoretical studies[11–13] showed distortion of the silicon diamond lattice structure that is related to lattice instability in the time scale of hundreds of femtoseconds following the ultrashort pulsed laser irradiation. Electronic excitation effects were suggested as the likely cause for the enhanced crystallization of amorphous GeSb films by laser pulses shorter than 800 fs.[14]

Rearrangement in atomic scale can be studied by probing with hard x-ray femtosecond pulses. Structural dynamics in femtosecond temporal resolution can then be measured, since the x-ray wavelength is comparable to the interatomic distance. Recently, solid evidence for nonthermal melting was achieved by femtosecond time-resolved x-ray probing.[15] Depletion of x-ray diffraction images at the irradiated areas signifies disordering of the crystal structure, while a nonthermal liquid layer is assumed to form homogeneously at laser fluences exceeding the respective transition threshold.

In this work, theoretical background on the laser interaction with a-Si film and the crystallization process is presented in Sec. 2. The experimental description follows in Sec. 3. Experimental results interrogating the phase transition process with time-resolved imaging in conjunction with postprocessing atomic force microscopy and scanning electron microscopy (AFM/SEM) measurements are given in Sec. 4. An optimal fluence for crystallization is identified.

2 Theoretical Consideration

Laser light first interacts with the electronic system during irradiation. Electrons absorb photons being excited into the higher energy band and leaving holes in the lower energy band dominantly by linear absorption and a two-photon absorption mechanism. Excited electron-hole pairs then thermalize very rapidly within a few tens of femtoseconds.[16] Ignoring intraband relaxation, recombination, and diffusion (this can be justified, since these processes are much slower than excitation), the conservation equation for energy carriers can be written as follows.

$$\frac{\partial N(x,t)}{\partial t}=\frac{(1-R)\alpha I(x,t)}{h\nu}+\frac{(1-R)^2\beta I^2(x,t)}{2h\nu}, \tag{1}$$

where R is the reflectivity (0.35),[17] α is the linear absorption coefficient ($4\pi\kappa/\lambda$, $2.36\times10^4\ \mathrm{cm}^{-1}$)[17] $h\nu$ is the en-

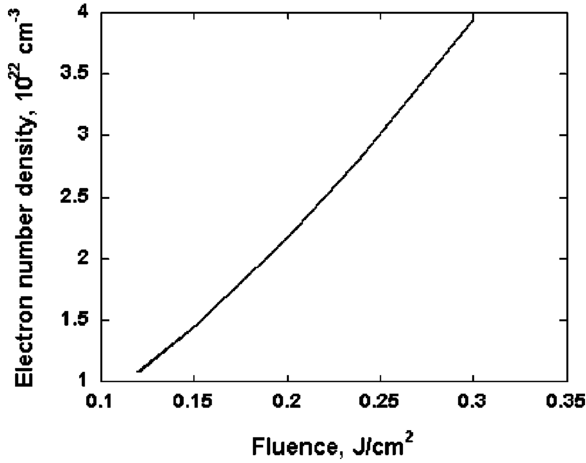

Fig. 1 Electron number density as a function of fluence. Note 10^{22} cm^{-3} is the theoretical lower limit of lattice instability.

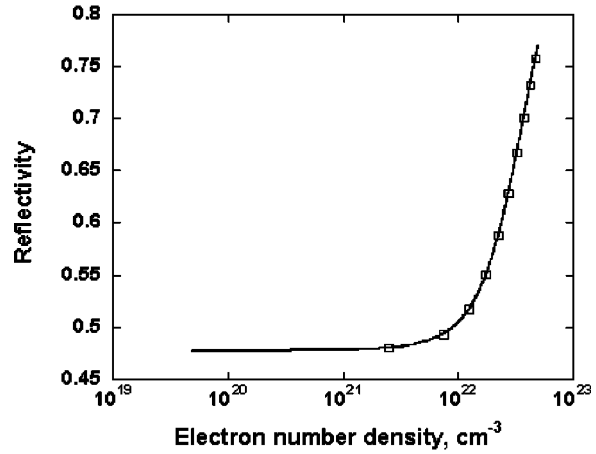

Fig. 2 Reflectivity as a function of electron number density. The probe light is normally incident on the sample at 400 nm.

ergy quantum of 800-nm wavelength light, β is the two photon absorption coefficient (37 cm/GW),[18] and $I(x,t)$ is the laser intensity expressed as follows.

$$\frac{\partial I(x,t)}{\partial x}=-(\alpha+\Theta N)I, \tag{2}$$

where Θ is the free-carrier absorption cross section (6×10^{-17} cm^2).[19]

The electron number density increases with excitation, and has peak value at the time around when the intensity is maximized. The density extends over 10^{22} cm^{-3} for all fluences, as indicated in Fig. 1. This density is at the lower limit of lattice instability.[11]

The Drude expression for the complex refractive index is introduced to estimate the transient reflectivity and predict the subpicosecond response of the a-Si film.[20]

$$n^c=\left[\varepsilon_{a\text{-}Si}-\left(\frac{\omega_p}{\omega}\right)^2\frac{1}{1-i\dfrac{1}{\omega\tau_d}}\right]^{1/2}, \tag{3}$$

where ω is the angular frequency of the probe light, τ_d is the damping time, $\varepsilon_{\text{a-Si}}$ is the dielectric constant of solid amorphous silicon $(13.4+i18.9)$,[17] and ω_p is the plasma frequency expressed as follows.

$$\omega_p=\frac{4\pi Ne^2}{m^*m_e}, \tag{4}$$

where m_e is the electron rest mass, and m^* is the ratio of electron effective mass to the mass at rest, taken as 0.18. The damping time is chosen at 1 fs, considering a high carrier-carrier collision rate.[21] The calculated surface reflectivity is plotted in Fig. 2. Lattice disorder is triggered beyond 10^{22} cm^{-3} as the reflectivity approaches that of liquid silicon ($R=0.72$ at the 400-nm probing laser light wavelength[22]).

When solid matter is heated past the melting point and subjected to a quenching process, heterogeneous nucleation is usually initiated at local defects and is followed by solidification and crystallization. Accordingly, nanosecond pulsed laser crystallization of a-Si films for the production of p-Si TFTs works via a thermally driven and melt-mediated phase transformation sequence.[23] The experimental results presented in the subsequent section show that the ultrafast phase transition imparted by femtosecond laser radiation and the ensuing thermal melting lead to crystallization of a-Si.

3 Experiment

The objective of the present work is to identify and investigate the fundamental mechanisms of phase transformations in amorphous solid matter at extremely fast rates. To accomplish this, 100-nm-thick amorphous-silicon (a-Si) films deposited by low-pressure chemical-vapor deposition (LPCVD) on quartz substrates were subjected to ultrafast laser pulses of full-width half-maximum (FWHM) duration of about 90 fs. The pulses were delivered at wavelength $\lambda=800$ nm, maximum energy of 1 mJ, and repetition rate of 1 kHz by a solid-state laser-pumped Ti:Al_2O_3 femtosecond oscillator seeding a regenerative amplifier. Scanning electron microscopy (SEM) as well as atomic force micros-

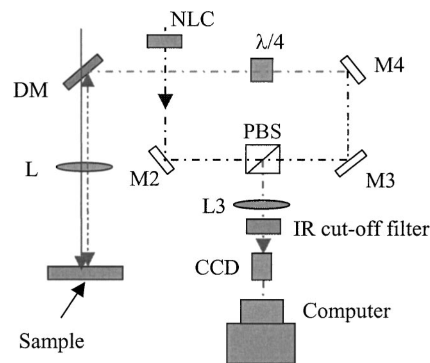

Fig. 3 Schematic diagram of the experimental setup. NLC is the nonlinear crystal, DM is the dichroic mirror, PBS is the polarizing beamsplitter, $\lambda/4$ is the quarter wave plate, M is the mirror, L is the lens. The solid line is a pump beam ($\lambda=800$ nm) and the dotted line is a probe beam ($\lambda=400$ nm).

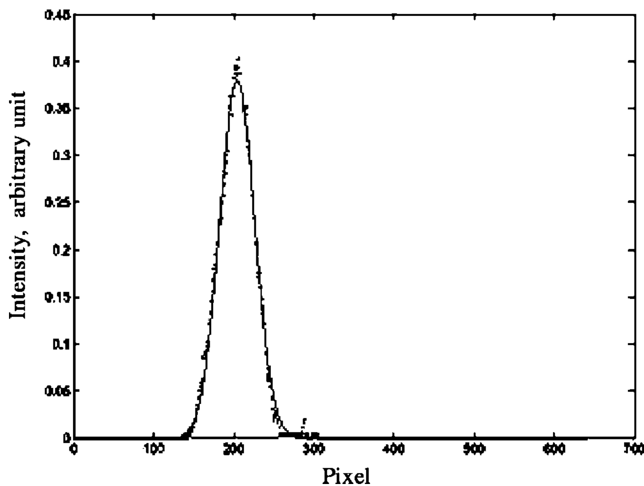

Fig. 4 Fiber-coupled probe beam across the imaging CCD camera, showing Gaussian profile.

copy (AFM) observation of the resulting material revealed recrystallization to a polycrystalline (p-Si) structure.

The dynamics of the rapid phase transformation are probed by ultrafast pump-and-probe imaging and reflectivity measurement. A schematic illustration of the experiment setup is given in Fig. 3. The first high-energy pump beam intercepts the sample surface at normal incidence. The energy is calibrated by using a precise energy meter. The average pulse energy was taken over 50 shots, with the deviation falling within 1% of the mean value. Focal spot size is determined by a knife-edge experiment. A second, lower power beam is split off the main beam, frequency-doubled to $\lambda = 400$ nm, and also directed at normal incidence onto the sample surface. The reflected probe beam is routed through various optical components to finally relay the image via a narrow bandpass interference filter centered at 400 nm to a CCD camera. The camera is connected to a digital image acquisition board of a personal computer. The acquired digitized image was then processed by software to extract the grayscale intensity distribution.

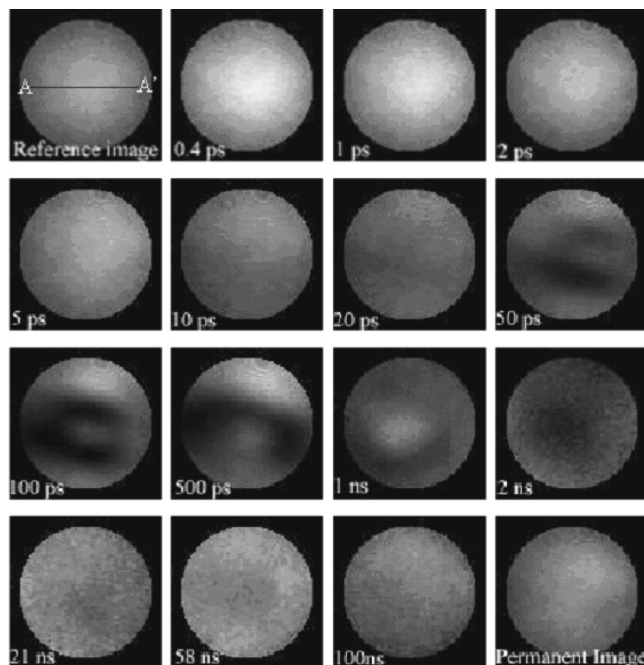

Fig. 5 Time-resolved images between 0.4 ps and 100 ns. The laser fluence was set at 0.12 J/cm^2. Rapid phase changes are recorded with optical reflection snap shots. Note that an optical fiber technique has been utilized beyond 1 ns.

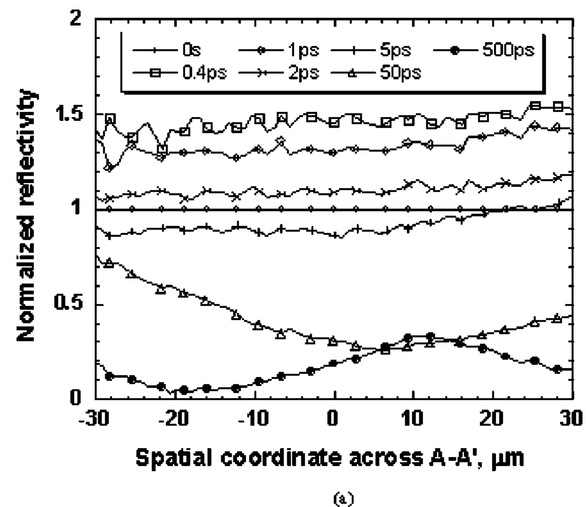

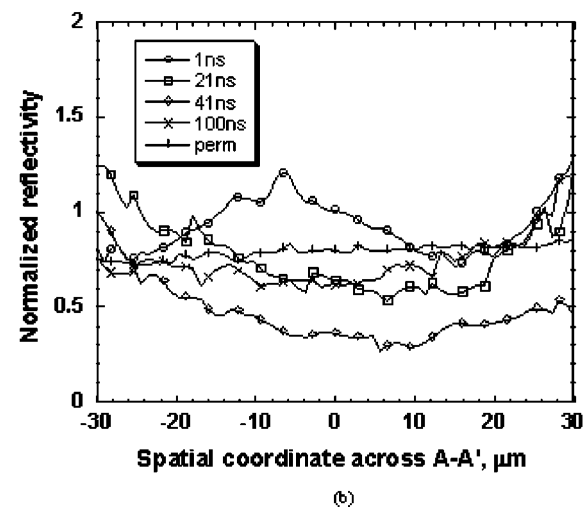

Fig. 6 Normalized reflectivity on the cross section A-A′ in Fig. 5: 1 represents no change. (a) 0.4 to 500 ps and (b) 1 ns-$t = \infty$.

The time delay between the main (pump) beam and the probe beam is adjusted by a precision translation stage for time delays shorter than 200 ps. To acquire images beyond 1 ns, the probe beam was guided through an optical fiber of variable length that was inserted between the nonlinear crystal (NLC) and mirror 2 (M2). This scheme allows extension of the time delay from a minimum of about 100 fs to the nanosecond regime. Beam coupling into the fiber optical component is critical for obtaining the smooth Gaussian profile shown in Fig. 4.

4 Results and Discussions

As discussed in Sec. 2, the lattice instability driven by high-density electron-hole plasma could be one mechanism for phase transformation. This plasma annealing mechanism is also detected via loss of the second harmonic generation

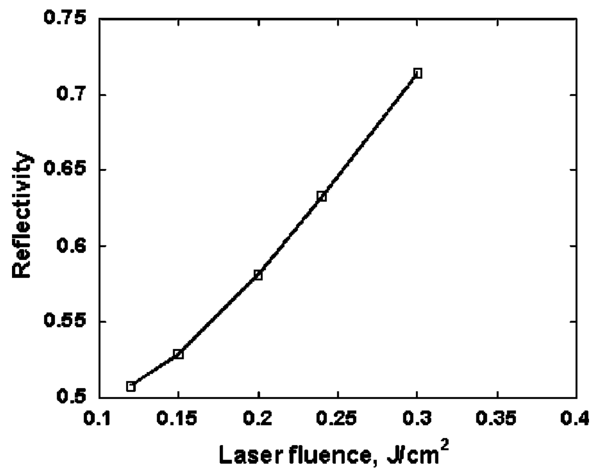

Fig. 7 Reflectivity as a function of laser fluence. Electron density is estimated by 1-D rate equation and Eqs. (3)–(4) are used.

(SHG).[8] A short-lived, nonthermal phase was detected in the subpicosecond time scale with reflectivity comparable to the liquid phase reflectivity.[10,24] A clear distinction of the transition between the ultrafast liquid phase and the electron-hole plasma state is difficult. Nevertheless, it is certainly true that the classical model of crystallization mediated by thermal melting cannot satisfactorily explain the subpicosecond rapid phase transition.

Images taken at different temporal delays are shown in Fig. 5. The initial bright images (0.2 to 1 ps) shown in Fig. 5 are ascribed to the nonthermal phase-change process. The normalized reflectivity in Fig. 6 is defined as $R_{\mathrm{norm}} = R_{\mathrm{trans}}/R_{\mathrm{ref}}$, where R_{trans} is the reflectivity response to the pump beam excitation, and R_{ref} represents the reference reflectivity of the pristine surface. The absolute reflectivity at early times is 0.66 to 0.71 by considering the normal-incidence reflectivity of the a-Si surface at 400 nm (0.47[16]), i.e., close to the reflectivity of liquid silicon at 400 nm. On the other hand, the predicted reflectivity on the basis of Eqs. (1) through (4) varies from 0.55 to 0.6 over the area irradiated by the Gaussian laser intensity distribution. The calculated reflectivity as a function of fluence at 400 fs is shown in Fig. 7. It is noted that the reflectivity at the early stage is constant through the cross section, implying that the reflectivity has no fluence (0 to 0.24 J/cm^2 in A-A′) dependence during the ultrafast phase change (up to a few picoseconds), thus meaning that the change might have occurred not only by electronic effects but also by lattice redistribution (see Figs. 1, 2, and 7 for reflectivity dependence on fluence).

Time-resolved x-ray diffraction probing experiments indicated that phase transitions excited at near-threshold fluence follow a thermal path.[15] This situation holds in the outskirts of the irradiated area where the local fluence drops according to the Gaussian beam profile. In contrast, a rapid homogeneous phase transformation emerges within the first picosecond, as shown in Fig. 5. It should be noted, however, that thermal melting can also occur in the solid beneath the nonthermally transformed surface layer.[15] The nonthermal phase vanishes after an elapsed time of a few picoseconds. The energy exchange between the electron and lattice systems is converted to phonon vibration by phonon relaxation within 10 ps.[25] The highly nonequilibrium state and defects formed in this process are suggested as the driving forces to subsequent rapid nucleation.

The dramatic reflectivity decrease observed between 50 and 500 ps may be caused by rapidly evolving surface features scattering the incident probe beam light. The reflectivity exhibits an oscillatory behavior from 500 ps to a few nanoseconds. The reflectivity rise to 0.6 at the center of the irradiated spot at $t=1$ ns (Fig. 6) is consistent with the formation of a very thin thermal melt layer.[7] This thin surface layer solidifies quickly, due to heat loss via conduction. The release of latent heat on the solidification process can then drive a buried melt layer, propagating through the thickness of the film via the so-called explosive crystallization mechanism.[26] The self-sustained explosive crystallization mechanism can contribute to the formation of polycrystals of ~50-nm average grain size observed in the SEM image, depicted in Fig. 8. As shown in the AFM

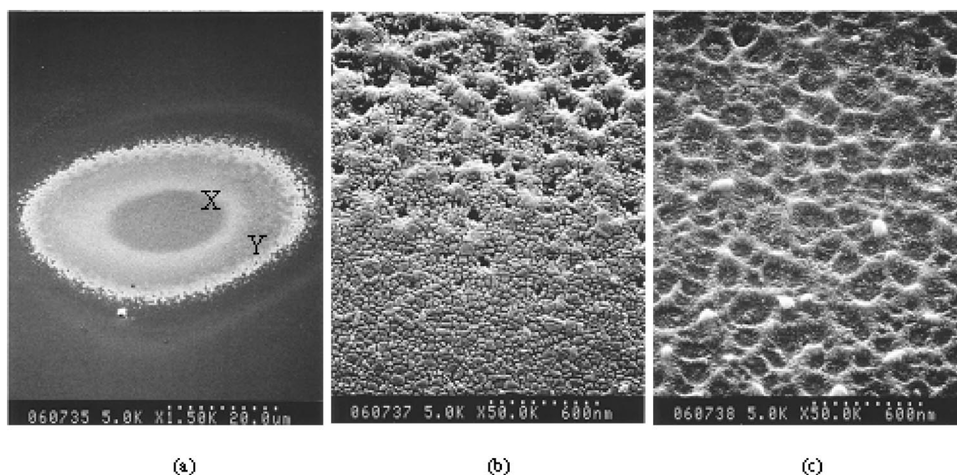

Fig. 8 SEM images of crystallization of a 100-nm-thick a-Si film on a quartz substrate by a single femtosecond laser pulse at fluence of 0.12 J/cm^2. (b) The higher magnification SEM depicts the transition zone [signified as X in (a)] to polycrystalline (p-Si) material. (c) The peripheral area does not show polycrystalline structures.

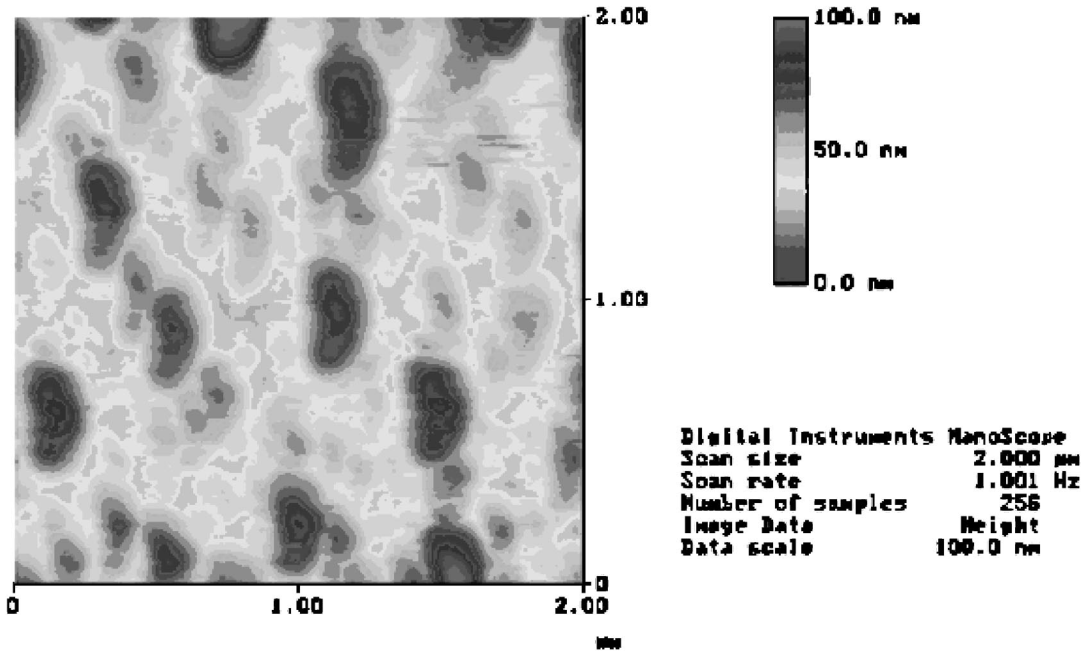

Fig. 9 AFM height image of the central area in Fig 8(a). Average grain size and height is about 50 nm.

measurement of Fig. 9, the induced peak surface roughness is about the same as the grain size.

SEM images in Fig. 10, corresponding to lower (80 mJ/cm^2) and higher (150 mJ/cm^2) laser energy density, do not show crystallization. Dispersed islands are produced at 80 mJ/cm^2 as shown in Fig. 10(a). On the other hand, the surface appears only roughened in Fig. 10(c), possibly due to release of particles from the surface, melt redistribution, and instability at the fluence of 150 mJ/cm^2. The fluence range for achieving effective crystallization is therefore narrow.

Since the reflection image at $t = 100$ ns is close to a steady state ($t = \infty$), it is concluded that the crystallization process is essentially completed by that time. It is noted that the absolute reflectivity remains lower than the pristine a-Si reflectivity and consistent with the polysilicon phase.

5 Summary

Ultrashort laser pulses are utilized to crystallize 100-nm-thick a-Si films, which can be a promising building block for fabricating thin film transistors (TFTs). The optimal laser fluence for crystallization of about 120 mJ/cm^2 yields grains of 50-nm average size. Femtosecond time-resolved pump-and-probe images are acquired to study the ultrafast phase change and crystallization process. Images taken at elapsed times shorter than 1 ps indicate phase transition mediated by a short-lived nonthermal lattice disorder. Defect formation of nucleation sites induced by this ultrafast

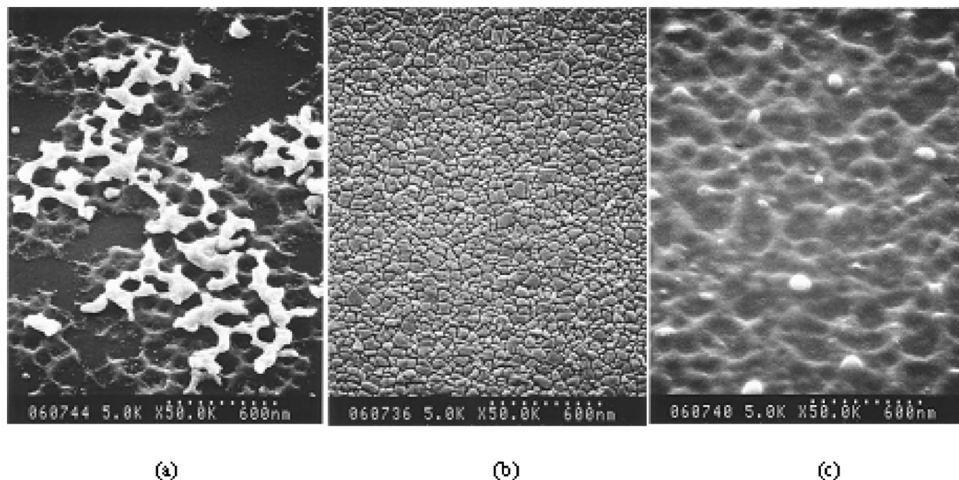

Fig. 10 Central area of the irradiated spot [Only case (b) shows crystallization]: (a) $F = 80$ mJ/cm^2, (b) $F = 120$ mJ/cm^2, and (c) $F = 150$ mJ/cm^2.

phase transition, followed by surface melting and explosive crystallization that evolve in the nanosecond temporal scale, are suggested as possible crystallization mechanisms. As an extension of this study, polycrystalline grain size and growth control by using additional beams and appropriate masks can be done.

Acknowledgment

Support of this work by the National Science Foundation under grant CTS-0074597, and by the Department of Energy, Office of Basic Energy Sciences, Engineering Research Program under grant DE-FG03-95ER14562 is gratefully acknowledged. Valuable discussion with Seungjae Moon is also acknowledged.

References

1. M. Lee, S. Moon, M. Hatano, and C. P. Grigoropoulos, "Ultra-large lateral grain growth by double laser recrystallization of a-Si films," *Appl. Phys.* **73**, 317–322 (2001).
2. M. Hatano, S. Moon, M. Lee, K. Suzuki, and C. Grigoropoulos, "*In situ* and *ex situ* diagnostics on melting and resolidification dynamics of amorphous and polycrystalline silicon thin films during excimer laser annealing," *J. Non-Cryst. Solids* **266–269**, 654–658 (2000).
3. D. von der Linde and N. Fabricius, "Observation of an electronic plasma in picosecond laser annealing of silicon," *Appl. Phys. Lett.* **41**, 991–993 (1982).
4. J. Van Vechten, R. Tsu, and F. Saris, "Nonthermal pulsed laser annealing of Si, plasma annealing," *Phys. Lett. A* **74A**, 422–426 (1979).
5. C. V. Shank, R. Yen, and C. Hirlimann, "Time-resolved reflectivity measurements of femtosecond-optical-pulse-induced phase transitions in silicon," *Phys. Rev. Lett.* **50**, 454–457 (1983).
6. M. C. Downer, R. L. Fork, and C. V. Shank, "Femtosecond imaging of melting and evaporation at a photoexcited silicon surface," *J. Opt. Soc. Am. B* **2**, 595–599 (1985).
7. K. Sokolowski-Tinten, J. Solis, J. Bialkowski, J. Siegel, C. N. Afonso, and D. von der Linde, "Dynamics of ultrafast phase changes in amorphous GeSb films," *Phys. Rev. Lett.* **81**, 3679–3782 (1998).
8. H. W. K. Tom, G. D. Aumiller, and C. H. Brito-Cruz, "Time-resolved study of laser-induced disorder of Si surfaces," *Phys. Rev. Lett.* **60**, 1438–1441 (1988).
9. D. Guidotti, T. A. Driscoll, and H. J. Gerritsen, "Second harmonic generation in centrosymmetric semiconductors," *Solid State Commun.* **46**, 337–340 (1983).
10. K. Sokoloski-Tinten, J. Bialkowski, and D. von der Linde, "Ultrafast laser-induced order-disorder transitions in semiconductors," *Phys. Rev. B* **51**, 14186–14198 (1995).
11. P. Stampfli and K. H. Bennemann, "Theory for the instability of the diamond structure of Si, Ge, and C induced by a dense electron-hole plasma," *Phys. Rev. B* **42**, 7163–7173 (1990).
12. P. Stampfli and K. H. Bennemann, "Dynamical theory of the laser-induced lattice instability of silicon," *Phys. Rev. B* **46**, 10686–10692 (1992).
13. P. L. Silvestrelli, A. Alavi, M. Parrinello, and D. Frenkel, "Ab initio molecular dynamics simulation of laser melting of silicon," *Phys. Rev. Lett.* **77**, 3149–3152 (1996).
14. J. Solis, C. N. Afonso, S. C. W. Hyde, N. P. Barry, and P. M. W. French, "Existence of electronic excitation enhanced crystallization in GeSb amorphous thin films upon ultrashort laser pulse irradiation," *Phys. Rev. Lett.* **76**, 2519–2522 (1996).
15. C. Siders, A. Cavalleri, K. Sokolowski-Tinten, C. Toth, T. Guo, M. Kammler, M. von Hoegen, K. Wilson, D. von der Linde, and C. Barty, "Detection of nonthermal melting by ultrafast X-ray diffraction," *Science* **286**, 1340–1342 (1999).
16. H. M. van Driel, "Kinetics of high-density plasmas generated in Si by 1.06-and 0.53-μm picosecond laser pulses," *Phys. Rev. B* **35**, 8166–8176 (1987).
17. E. Palik, *Handbook of Optical Constants of Solids*, Academic Press, New York (1985).
18. A. Haché and M. Bourgeois, "Ultrafast all-optical switching in a silicon-based photonic crystal," *Appl. Phys. Lett.* **77**, 4089–4091 (2000).
19. A. Bugaev, O. Kon'kov, and E. Terukov, "Nonlinear absorption of a picosecond pulse in a-Si:H," *Phys. Solid State* **42**, 241–243 (2000).
20. M. Born and E. Wolf, *Principles of Optics*, Cambridge University Press, Boston, MA (1999).
21. K. Sokolowski-Tinten and D. von der Linde, "Generation of dense electron-hole plasmas in silicon," *Phys. Rev. B* **61**, 2643–2650 (2000).
22. G. Jellison Jr. and D. Lowndes, "Measurement of the optical properties of liquid silicon and germanium using nanosecond time-resolved ellipsometry," *Appl. Phys. Lett.* **51**, 352–354 (1987).
23. T. Dyer, J. Marshall, W. Pickin, A. Hepburn, and J. Davies, *J. Non-Cryst. Solids* **164–166**, 1001 (1993).
24. L. Huang, J. Callan, E. Glezer, and E. Mazur, *Phys. Rev. Lett.* **80**, 185 (1998).
25. D. Von der Linde, J. Kuhl, and H. Klingenberg, "Raman scattering from nonequilibrium LO phonons with picosecond resolution," *Phys. Rev. Lett.* **44**, 1505–1508 (1980).
26. K. Murakami, O. Eryu, K. Takita, and K. Masuda, "Explosive crystallization starting from an amorphous-silicon surface region during long-pulse laser irradiation," *Phys. Rev. Lett.* **59**, 2203–2206 (1987).

Tae Y. Choi received his PhD from University of California (UC), Berkeley, in 2002. His main research topic during the PhD program was femtosecond laser-induced micro/nano-fabrication. After being a postdoctoral researcher in the Laser Thermal Laboratory of UC Berkeley for a short period, he joined the Laboratory of Thermodynamics in Emerging Technologies at ETH Zurich, Switzerland, as a senior scientist. He is interested in various topics including micro/nano-scale phase transformation using AFM and neer-field scanning optical microscopy (NSOM).

David J. Hwang received his BSc (1995) and MSc (1997) degree in Mechanical engineering from Seoul National University, South Korea. From 1997 to 2000, he worked for Samsung Advanced Institute of Technology, South Korea, his research concerning automotive engine control, cryogenic cooling of superconductors and microscale jetting devices. Since 2000, he has been working as a graduate student researcher in the Department of Mechanical Engineering at the University of California, Berkeley. His research interests are micro/nano-scale modification by ultrashort lasers and AFM/NSOM.

Costas P. Grigoropoulos received his Diploma degrees in naval architecture and marine engineering (1978), and in mechanical engineering (1980) from the National Technical University of Athens, Greece. He holds a MSc degree (1983), and a PhD (1986), both in mechanical engineering from Columbia University. He joined the faculty of the Department of Mechanical Engineering at the University of California at Berkeley as an assistant professor in 1990, after serving as an assistant professor of mechanical engineering at the University of Washington from 1986 to 1990. He was promoted to associate professor in mechanical engineering in July 1993 and to professor in mechanical engineering in July 1997. He is a Fellow of the American Society of Mechanical Engineers and an Associate Editor for the *Journal of Heat Transfer* and the *International Journal of Heat and Mass Transfer*. His research interests are in laser materials processing, and micromachining, radiative and thermal properties of thin film materials, laser-induced thin film crystal growth for large area electronics, microscale and nanoscale flow, mass, energy transport and surface engineering, and ultra-fast laser interactions with materials. He has established the Laser Thermal Laboratory for the study of rapid phase-change phenomena in materials processing, and for developing innovative approaches for thermal management in microsystems. A variety of experimental techniques are utilized for probing microscopic transport phenomena and testing miniature devices, including femtosecond time-resolved imaging and spectroscopy, noncontact fast temperature measurement via multicolor pyrometry, microparticle imaging velocimetry (PIV), thermal velocimetry, laser-induced fluorescence, absorption imaging, mass spectroscopy, emission spectroscopy, interferometry, and high-speed visualization. Experimental work is also being carried out on nanoscale surface modification and probing of transport phenomena using NSOM in both apertureless and fiber coupled modes.